A Laser System Model for Enhanced Operational Performance and Flexibility on OMEGA EP

M. J. Guardalben, M. Barczys, B. E. Kruschwitz, M. Spilatro, L. J. Waxer, and E. M. Hill

Laboratory for Laser Energetics, University of Rochester

Introduction

The ability of high-energy laser systems to provide complex laser pulse shapes has growing importance in many research disciplines such as laser fusion,[1–4] high-energy-density physics,[5–8] laboratory astrophysics,[9–11] and laser conditioning of optical materials.[12] For example, x-ray diffraction of ramp-compressed crystalline solids can probe high-pressure phase transitions inaccessible with shock compression.[6] In such laser facilities, accurate, real-time predictions of laser performance are critical for maximizing experimental and operational effectiveness and flexibility. Several laser operations models that predict laser performance for high-energy laser systems have been reported.[13–22] Most of these models utilize optimization methods that comprise forward-propagation simulations with feedback to converge on the required on-target pulse power. This article reports on *PSOPS*—a MATLAB[23]-based semi-analytic model developed for the OMEGA EP[24] Laser System. *PSOPS* provides rapid and accurate predictions of OMEGA EP Laser System performance in both forward and backward directions, a user friendly interface, and rapid optimization capability between shots. The model's features have allowed real-time optimization of the laser system configuration in order to satisfy the demands of rapidly evolving experimental campaign needs and have enabled several enhancements to the accuracy and flexibility of laser system performance.

Functional Overview of *PSOPS*

The backward simulation capability of the model is used in the configuration of the system for a shot where the desired UV energy, pulse shape, expected beam profile, and beamline amplifier configuration are provided as inputs to the *PSOPS* model. The results are the required pulse shape at the input of the system, as well as the energies at each stage of the laser, from which the laser throttles and diagnostic configurations can be determined in a fast and robust manner.

During shot operations, *PSOPS* is used in the forward simulation direction to provide rapid predictions of laser-system performance using measured inputs to the amplifier chain. The measured input beam profile and real-time–measured input pulse shape are used with the expected beamline injected energy and previously measured beamline small-signal gain to predict the IR and frequency-converted UV performance at the end of the beamline. A front-end qualification shot is taken at the start of a shot day to confirm the expected injected energy and to measure the injected beam near-field distribution that is used as input to the *PSOPS* model.

Laser pulse shape, energy, and near-field beam profile are measured at several locations along the beam path. Diagnostic stages relevant to the *PSOPS* model and associated measurements are shown in Fig. 1. The output pulse shape of each beamline's regenerative amplifier is measured at a 5-Hz repetition rate using a photodiode-based pulse-stacking, pulse-shape monitor (PSM).[25] Calorimetrically calibrated charge-coupled–device (CCD) cameras (Scientific Instruments, model SI-800) are used to measure the beam's near-field profile and laser-beam energy at the beamline injection and amplified beamline output stages. A harmonic energy diagnostic (HED)[26] is used to measure the UV energy and the residual green and IR energy of the frequency-converted laser beam. Amplified IR and UV pulse shapes are measured using ROSS streak cameras.[27] These diagnostic measurements are used to calibrate the *PSOPS* model and also to determine the required stage energies and pulse shapes in both forward and backward directions when configuring for a shot.

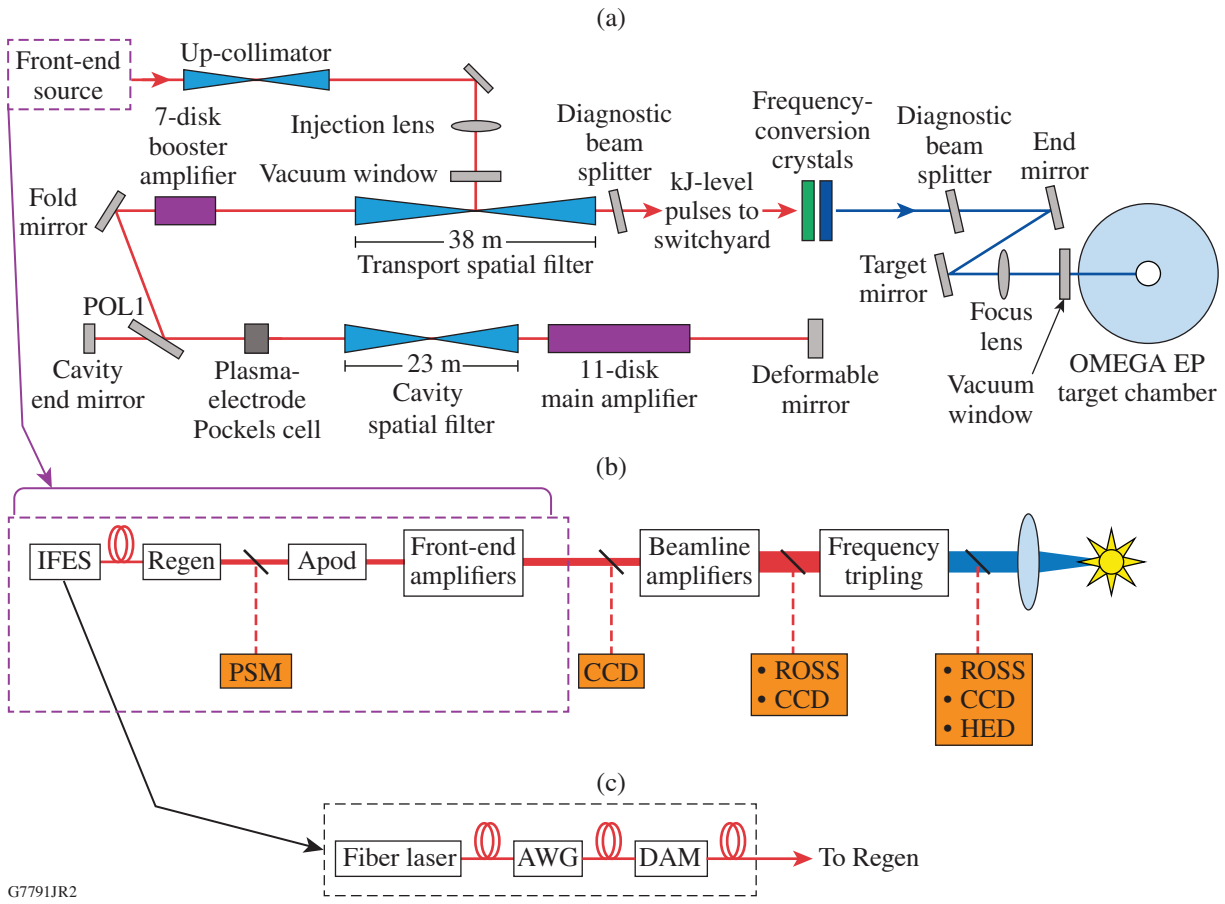

Figure 1
(a) Configuration of an OMEGA EP beamline. (b) Block diagram of (a) showing locations of pulse-shape, beam-profile, and energy-measurement diagnostics used with the *PSOPS* model. PSM: pulse-shape monitor; Apod: beam-shaping apodizer; CCD: near-field charge-coupled–device camera; ROSS: Rochester optical streak system; and HED: harmonic energy diagnostic. (c) An integrated front-end system (IFES) produces temporally shaped, 1053-nm pulses from a single-frequency, continuous-wave (cw) fiber laser. Precisely shaped temporal pulses are formed using an arbitrary waveform generator (AWG) that drives a dual-amplitude modulator (DAM).

PSOPS Model Description

Analytic solutions to the four-level, coupled-rate, and energy-transport equations for a homogeneously saturating thin slab[28] are used in *PSOPS* to determine the time-dependent gain within each LHG-8, Nd-doped laser disk at discrete locations across the laser aperture. For multipass amplification in the forward propagation direction, the output intensity of disk k is given by

$$I_k(t,x,y) = \beta^2 \cdot G_k(t,x,y) I_{k-1}(t,x,y), \tag{1}$$

where

$$G_k(t,x,y) = \frac{1}{1-\left\{1-\left[G_0(x,y)\right]^{-1}\right\}\exp\left[-F_k(t,x,y)/F_{\text{sat}}\right]}, \tag{2}$$

$$F_k(t,x,y) = \int_{t_0}^{t} \beta \cdot I_{k-1}(t',x,y)\,\mathrm{d}t', \tag{3}$$

where G_0 is the small-signal gain of the laser disk, F_{sat} is the saturation fluence, and a per-disk-surface loss factor β is included in the model to account for passive losses. The integral in Eq. (3) is taken in the frame of the laser pulse from the starting time of the pulse, t_0, up to the time t within the pulse. Following the repeated application of Eqs. (1)–(3) through the entire beamline, frequency conversion to the third harmonic uses look-up tables from *MIXER* calculations.[29,30] For backward prediction starting with the UV beam profile, pulse shape, and energy, these tables provide the amplified IR intensity at the end of the beamline from which the beamline input intensity is recursively calculated using Eqs. (4)–(6):

$$I_k(t,x,y) = I_{k+1}(t,x,y) \Big/ \beta^2 \cdot G_k(t,x,y), \tag{4}$$

$$G_k(t,x,y) = 1 + \left[G_0(x,y) - 1\right] \exp\left[-F_k(t,x,y) \Big/ F_{sat}\right], \tag{5}$$

$$F_k(t,x,y) = \int_{t_0}^{t} \left[I_{k+1}(t',x,y) \Big/ \beta\right] dt', \tag{6}$$

where $I_k(t,x,y)$ is the *input* intensity of the kth disk. The effective saturation fluence of the OMEGA EP beamline has been inferred from prior fits to gain-saturation data and takes into account an inhomogeneous broadening effect in the laser glass[31] and bottlenecking of the terminal level of the lasing transition for pulse widths close to the terminal-level lifetime τ_{10}, where $\tau_{10} \sim 0.25$ ns for Nd-doped phosphate laser glasses.[32,33]

Comparison of Experimental and Model Data

Spatial and temporal simulations in both forward and backward directions are in excellent agreement with measurements, as shown in Figs. 2 and 3.

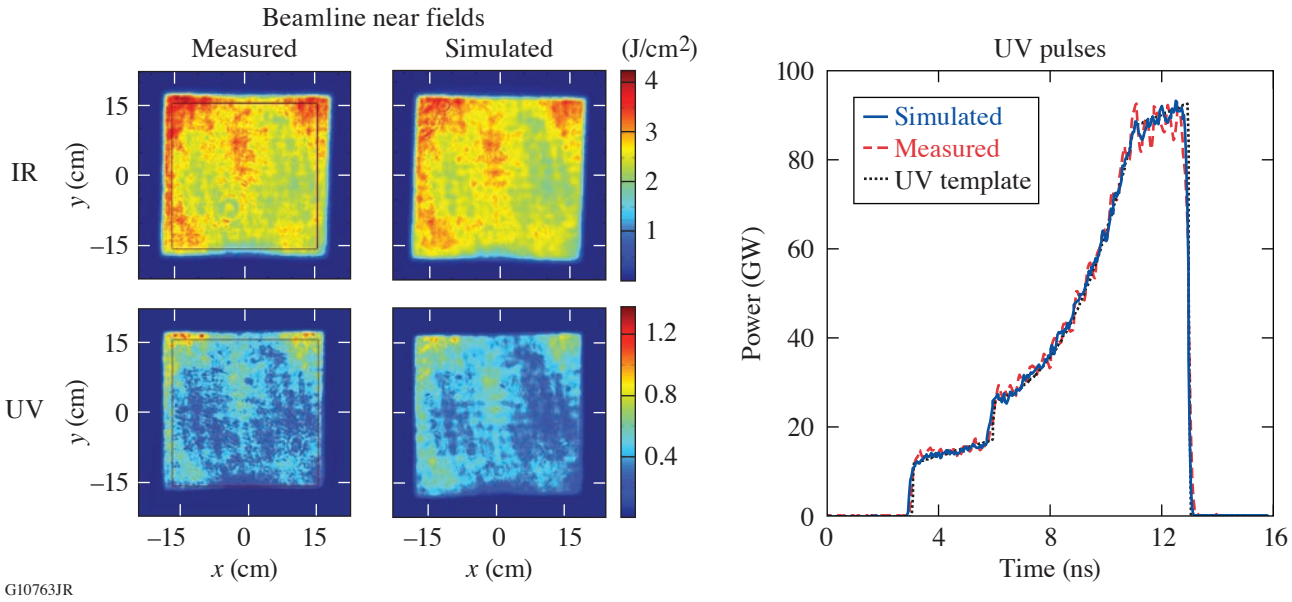

Figure 2
Comparison of *PSOPS* forward-simulated beam near fields, pulse shapes, and corresponding energies with measurements for Beamline 3, shot 20678. The forward simulation used the measured injected beam profile, pulse shape, and energy for shot 20678. IR: 3112 J measured; 3102 J simulated. UV: 453 J measured, 452 J simulated.

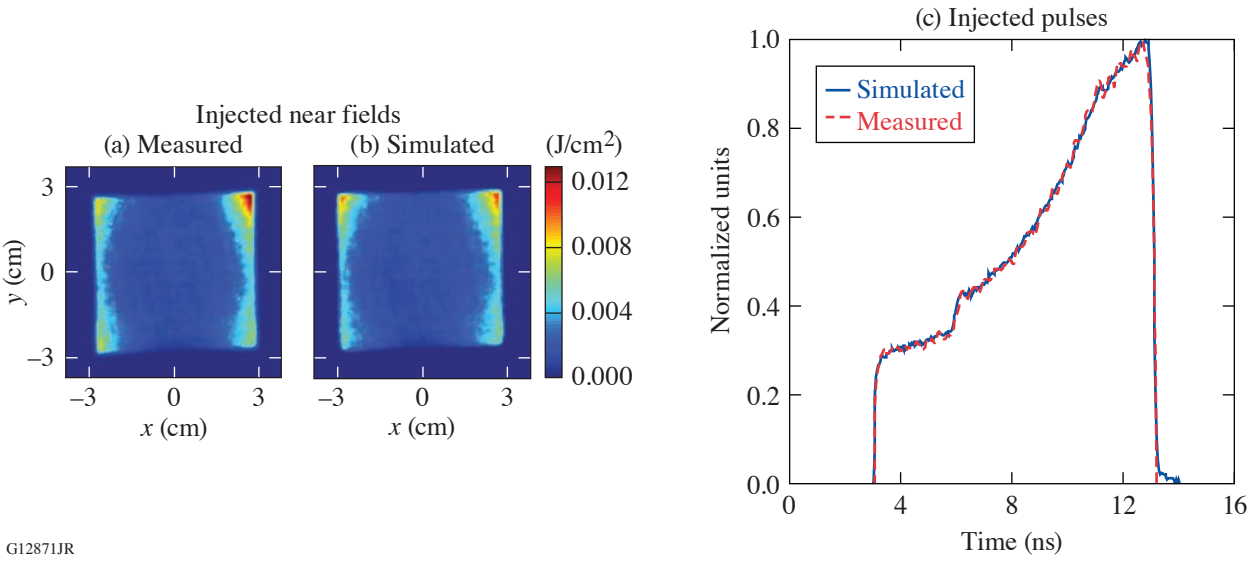

Figure 3
Comparison of *PSOPS* backward-simulated injected near-field beam profile, pulse shape, and energy with measurements for Beamline 3, shot 20678: (a) 79.5 mJ measured and (b) 76.9 mJ simulated. The backward simulation used the measured UV beam, pulse shape, and energy.

OMEGA EP Enhancements Enabled by *PSOPS*

1. Improvements to UV Energy and Pulse-Shape Accuracy

Drifts in system performance can lead to noticeable deviations between simulated and achieved pulse shapes and energies, which can be minimized with an agile system model such as *PSOPS*. For example, Fig. 4 shows how the injected pulse shape can be optimized for small changes in system performance. Figure 4(a) shows a pre-shot prediction on shot day that departs from the ideal pulse shape near the end of the pulse. Based on this prediction, the input pulse shape was modified to provide the compensated pre-shot prediction shown in Fig. 4(b). The post-shot UV simulation showed excellent agreement with the measurement [Fig. 4(c)].

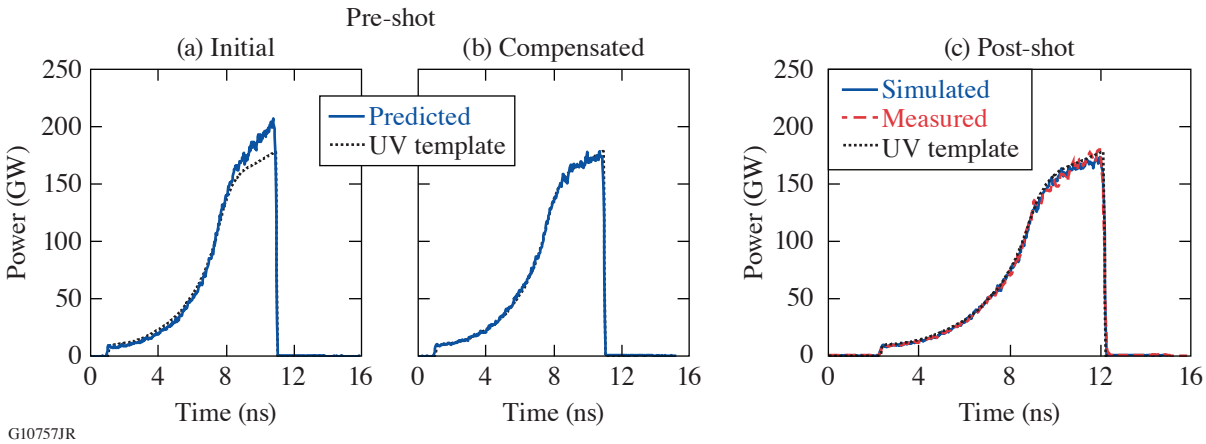

Figure 4
Predicted and requested UV pulse shapes showing how day-to-day changes in laser system performance are compensated using *PSOPS* predictions: (a) initial; (b) compensated; and (c) post-shot UV pulse simulation and measurement. On-target UV energy: 775 J requested, 751 J measured, 752 J simulated.

2. Improvements to Experimental Flexibility

PSOPS has also enhanced laser facility flexibility by enabling users to adjust requested UV pulse shapes and energies between laser shots, within a predefined range that is determined uniquely for each experimental campaign. The allowed range of energy and pulse-shape modification is assessed with respect to the laser system's fluence limits, the range of energy and pulse shapes planned for the day, and the likelihood of maintaining each beamline's 90-min shot cycle. In the example shown in Fig. 5, different energies were desired while maintaining the original normalized design pulse shape that produced 500 J of UV on-target energy. This request was accommodated in each case by adjusting the front-end pulse shape and throttles per the *PSOPS* pre-shot prediction.

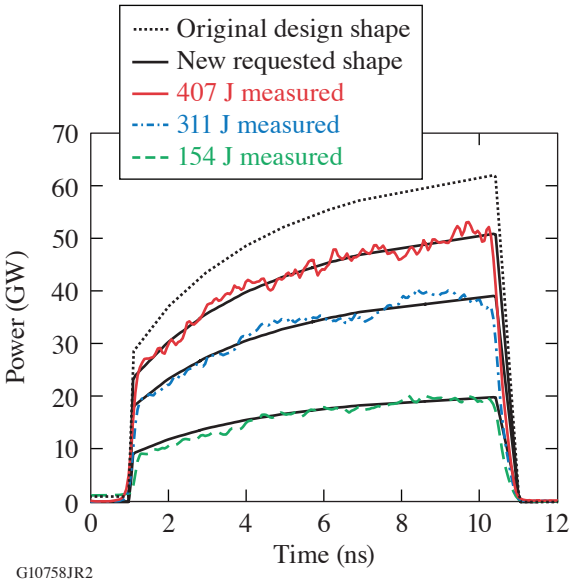

Figure 5
Example showing facility flexibility enabled by *PSOPS*. Based on a user's real-time analysis of experimental data, different energies were requested while maintaining the original normalized design pulse shape that produced 500-J on-target energy. The measured UV on-target energies are shown in the label.

3. Increased Effective Pulse-Duration Range

Currently, OMEGA EP can accommodate single-beamline pulse widths of up to 10 ns. However, improved system modeling in conjunction with precision timing allow the technique of pulse stitching to achieve up to a 4× increase in effective pulse duration. With pulse stitching, as illustrated in Fig. 6, pulse shapes from different beamlines can be precisely combined on target to form

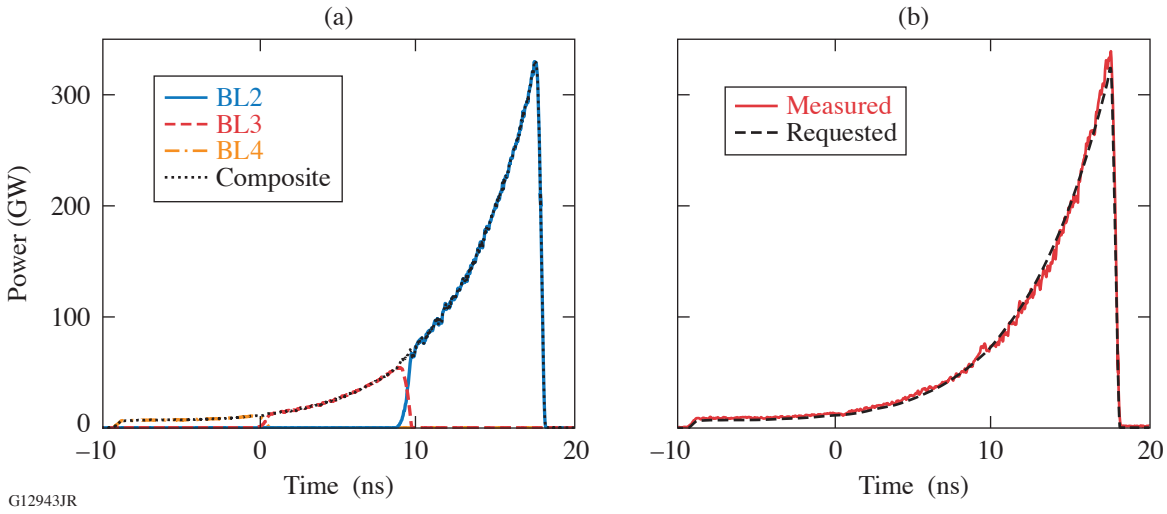

Figure 6
(a) Pre-shot prediction and (b) post-shot measurement of approximately 27-ns composite pulse shape formed by incoherent addition of the individual beamline pulse shapes and beam-to-beam timing (shot 31182).

a single composite pulse shape. In Fig. 6, the composite 27-ns ramped pulse shape shown was formed by incoherent addition of the individual pulses, separated by the temporal delay between them. Prior to the shot, *PSOPS* is used to predict the composite pulse given the specified beam-to-beam temporal delay [Fig. 6(a)]. The measured composite pulse shown in Fig. 6(b) was formed using the individual-beamline pulse-shape measurements and the measured beam-to-beam UV pulse timing.

4. Improved System Alignment

PSOPS has been used as a tool to optimize the alignment of beam-shaping apodizers[34] in the beamline front end. *PSOPS* predictions of the effect of small changes in beam centering and rotation on the amplified near-field beam uniformity can be used as a guide in the optimization of the apodizer alignment without requiring amplified shots. This has resulted in a better understanding of required tolerances for centering and rotation of both the beam-shaping apodizer and the apodized injected beam with respect to the gain profile of the beamline. As an example, Fig. 7 shows the measured effect that identifying and correcting a small error in apodizer alignment has on the amplified IR near-field beam. Using the measured injected near-field beam, *PSOPS* forward simulations were used to predict the amplified beamline output near-field profile and to correct the apodizer's alignment with respect to the gain profile of the beamline within a 10-min shot cycle. A 0.49-mm shift of the apodizer resulted in significantly improved beamline output near-field contrast and peak-to-mean fluence, as shown in Fig. 7(b). Contrast is defined as the standard deviation of the fluence divided by the mean fluence value. By limiting near-field beam fluence, fluence-limited damage may be avoided, leading to enhanced energy performance. In addition, these simulations have demonstrated that small adjustments to apodizer alignment are often sufficient to correct near-field beam nonuniformity in lieu of designing and manufacturing new apodizers.

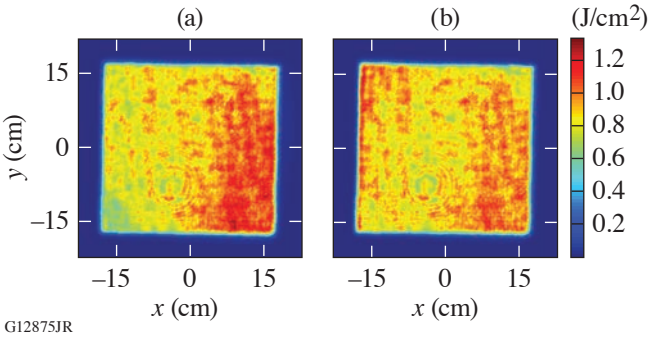

Figure 7
Measured Beamline 3 amplified IR output near-field profile (a) before moving the beam-shaping apodizer (contrast = 13.1%, peak-to-mean = 1.46:1) and (b) after moving the apodizer by 0.49 mm (contrast = 9.4%, peak-to-mean = 1.43:1). Contrast is defined in the text. The apodizer adjustment was guided by *PSOPS* simulations.

Summary

PSOPS is a semi-analytic model that is used on OMEGA EP to predict pulse shapes, stage energies, and near-field beam profiles in both forward and backward directions and has enabled accurate and rapid optimization of the laser system's performance within a small fraction of the OMEGA EP 90-min shot cycle. *PSOPS* is the key enabler of an automated capability to compute and specify the laser system's stage energies and corresponding system configurations prior to each OMEGA EP shot based upon evolving on-target pulse shape and energy requirements. The ability to calibrate the model between laser shots accounts for day-to-day system drifts without loss of shot time. Several facility enhancements have been enabled by *PSOPS*, such as improvements to UV energy and pulse-shape accuracy, improvements to experimental flexibility, increased effective pulse-duration range, and improved system alignment. An upgrade to the model currently in progress accounts for the spectral dependence of beamline gain and saturation fluence for shots that require spectrally tunable UV on-target irradiation to mitigate cross-beam energy transfer.[35]

This material is based upon work supported by the Department of Energy National Nuclear Security Administration under Award Number DE-NA0003856, the University of Rochester, and the New York State Energy Research and Development Authority.

1. S. X. Hu *et al*., Phys. Plasmas **25**, 082710 (2018).
2. D. Cao *et al*., Phys. Plasmas **25**, 052705 (2018).
3. J. Trela *et al*., Phys. Plasmas **25**, 052707 (2018).
4. A. Bose *et al*., Phys. Plasmas **25**, 062701 (2018).

5. M. Millot *et al*., Nature **569**, 251 (2019).
6. D. N. Polsin *et al*., Phys. Plasmas **25**, 082709 (2018).
7. D. N. Polsin *et al*., Phys. Rev. Lett. **119**, 175702 (2017).
8. M. C. Gregor *et al*., Phys. Rev. B **95**, 144114 (2017).
9. D. E. Fratanduono *et al*., Phys. Rev. B **97**, 214105 (2018).
10. R. F. Smith *et al*., Nat. Astron. **2**, 452 (2018).
11. F. Coppari *et al*., Nat. Geosci. **6**, 926 (2013).
12. K. R. P. Kafka, S. Papernov, and S. G. Demos, Opt. Lett. **43**, 1239 (2018).
13. M. J. Shaw *et al*., Opt. Eng. **43**, 2885 (2004).
14. M. J. Shaw *et al*., Proc. SPIE **5178**, 194 (2004).
15. R. A. Sacks *et al*., J. Phys.: Conf. Ser. **112**, 032024 (2008).
16. M. Shaw *et al*., J. Phys.: Conf. Ser. **112**, 032022 (2008).
17. D. I. Hillier, D. N. Winter, and N. W. Hopps, Appl. Opt. **49**, 3006 (2010).
18. B. J. Le Garrec and O. Nicolas, J. Phys.: Conf. Ser. **112**, 032019 (2008).
19. D. Hu *et al*., Chin. Opt. Lett. **13**, 041406 (2015).
20. K. T. Vu *et al*., Opt. Express **14**, 10,996 (2006).
21. W. Shaikh *et al*., *Central Laser Facility Annual Report 2005/2006*, 199, Rutherford Appleton Laboratory, Chilton, Didcot, Oxon., England (2005).
22. K. P. McCandless *et al*., in *Proceedings of the 14th International Conference on Accelerator & Large Experimental Physics Control Systems (ICALEPCS 2013)*, edited by C. Marshall, J. Fisher, and V. R. W. Schaa (The Joint Accelerator Conferences Website, Geneva, Switzerland, 2014), pp. 1426–1429.
23. MATLAB® R2013b, The MathWorks Inc., Natick, MA 01760-2098.
24. J. H. Kelly *et al*., J. Phys. IV France **133**, 75 (2006).
25. J. R. Marciante, W. R. Donaldson, and R. G. Roides, IEEE Photonics Technol. Lett. **19**, 1344 (2007).
26. *LLE Review Quarterly Report* **63**, 110, Laboratory for Laser Energetics, University of Rochester, Rochester, NY, LLE Document No. DOE/SF/19460-91 (1995).
27. W. R. Donaldson *et al*., Rev. Sci. Instrum. **73**, 2606 (2002).
28. A. E. Siegman, in *Lasers* (University Science Books, Mill Valley, CA, 1986), Chap. 10.
29. R. S. Craxton, Opt. Commun. **34**, 474 (1980).
30. R. S. Craxton, IEEE J. Quantum Electron. **QE-17**, 1771 (1981).
31. D. M. Pennington, D. Milam, and D. Eimerl, Proc. SPIE **3047**, 630 (1997).
32. C. Bibeau, J. B. Trenholme, and S. A. Payne, IEEE J. Quantum Electron. **32**, 1487 (1996).
33. C. Bibeau and S. A. Payne, 119, Lawrence Livermore National Laboratory, Livermore, CA, Report UCRL-LR-105820-95 (1996).
34. C. Dorrer and J. Hassett, Appl. Opt. **56**, 806 (2017).
35. B. E. Kruschwitz *et al*., Proc. SPIE **10898**, 1089804 (2019).